High-speed mid-infrared hyperspectral imaging using quantum cascade lasers[1]

David B. Kelley[a], Anish K. Goyal[a,2], Ninghui Zhu[a], Derek A. Wood[a], Travis R. Myers[a], Petros Kotidis[a], Cara Murphy[b], Chelsea Georgan[b], Gil Raz[b], Richard Maulini[c], and Antoine Müller[c]

[a]Block MEMS, 377 Simarano Drive, Marlborough, MA 01752;
[b]Systems & Technology Research, 600 West Cummings Park, Woburn, MA 01801;
[c]Alpes Lasers, Avenue des Pâquiers 1, 2072 St Blaise, Switzerland

ABSTRACT

We report on a standoff chemical detection system using widely tunable external-cavity quantum cascade lasers (EC-QCLs) to illuminate target surfaces in the mid infrared (λ = 7.4 – 10.5 μm). Hyperspectral images (hypercubes) are acquired by synchronously operating the EC-QCLs with a LN_2-cooled HgCdTe camera. The use of rapidly tunable lasers and a high-frame-rate camera enables the capture of hypercubes with 128 x 128 pixels and >100 wavelengths in <0.1 s. Furthermore, raster scanning of the laser illumination allowed imaging of a 100-cm^2 area at 5-m standoff. Raw hypercubes are post-processed to generate a hypercube that represents the surface reflectance relative to that of a diffuse reflectance standard. Results will be shown for liquids (e.g., silicone oil) and solid particles (e.g., caffeine, acetaminophen) on a variety of surfaces (e.g., aluminum, plastic, glass). Signature spectra are obtained for particulate loadings of RDX on glass of <1 μg/cm^2.

Keywords: Mid-IR spectroscopy, Quantum cascade laser, Hyperspectral imaging, Chemical detection, HgCdTe focal plane array

1. INTRODUCTION

Mid-infrared (MIR) spectroscopy has been identified as one of the most promising methods for standoff chemical detection due to the fact that most substances have strong and unique absorption features in the MIR spectrum [1-4]. Operating in the MIR enables rapid measurements while remaining below the eye-safety maximum-permissible-exposure limit of 100 mW/cm^2. When detecting remote chemical traces, it is often required to locate and identify the trace chemical within a larger scene necessitating high-spatial-resolution hyperspectral imaging (HSI). HSI is broadly defined as the capture of a series of images of a particular scene at a number of different wavelengths, typically with the intent to identify objects of interest within the scene. A hyperspectral image (hypercube) contains a wavelength spectrum for each pixel of the camera and represents a spectral map of the imaged surface. While some MIR spectroscopy systems rely on passive illumination of the scene by, e.g., the sun or thermal emission, much higher sensitivity is available through active illumination.

In order for an HSI system to capture specific wavelengths in a hypercube, there must be wavelength selection either in the illuminator or in the receiver. In this work, we use a widely-tunable EC-QCL which provides wavelength selection in the illuminator. EC-QCLs are a technology that has recently made significant advances in power output, spectral range, and tuning speed. They are commercially available in wavelengths that cover the range of 4 to 13 μm. They offer a rapidly tunable illumination source which can be combined with a high-speed, broadband HgCdTe (MCT) camera to capture spectral information rapidly and efficiently [5]. External-cavity interband cascade lasers (EC-ICLs) can also be used to extend the wavelength range of a MIR spectroscopy system to shorter wavelengths [6].

[1] This research was funded by the Office of the Director of National Intelligence (ODNI), Intelligence Advanced Research Projects Activity (IARPA), through the AFRL contract FA8650-16-C-9107. All statements of fact, opinion or conclusions contained herein are those of the authors and should not be construed as representing the official views or policies of IARPA, the ODNI, or the U.S. Government. The Government is authorized to reproduce and distribute reprints for Governmental purposes notwithstanding any copyright annotation thereon.
[2] Corresponding author: anish.goyal@blockeng.com.

Chemical, Biological, Radiological, Nuclear, and Explosives (CBRNE) Sensing XVIII, edited by Augustus Way Fountain III, Jason A. Guicheteau, Proc. of SPIE Vol. 10183, 1018304 · © 2017 SPIE
CCC code: 0277-786X/17/$18 · doi: 10.1117/12.2261851

The use of a wavelength tunable source in combination with a broadband receiver has several advantages over alternative methods:

- Photon-efficiency: Alternative approaches that use a spectrometer at the receiver (e.g., dispersive, interferometric) suffer from higher optical losses.
- Spatial resolution: Simple receive optics and an off-the-shelf broadband camera provide high resolution.
- Spectral specificity: Lasers can rapidly tune to any chosen wavelength, enabling the measurement of only those wavelengths that provide optimal discrimination and making efficient use of laser, camera, and computational resources.
- Modularity: With further advances in laser technology (e.g., power, tuning speed, spectral coverage, spectral resolution) and camera technology (e.g., frame rate, resolution), the overall system performance can be enhanced in a straightforward manner.

This paper presents details of our hyperspectral imaging system along with measurements and analysis.

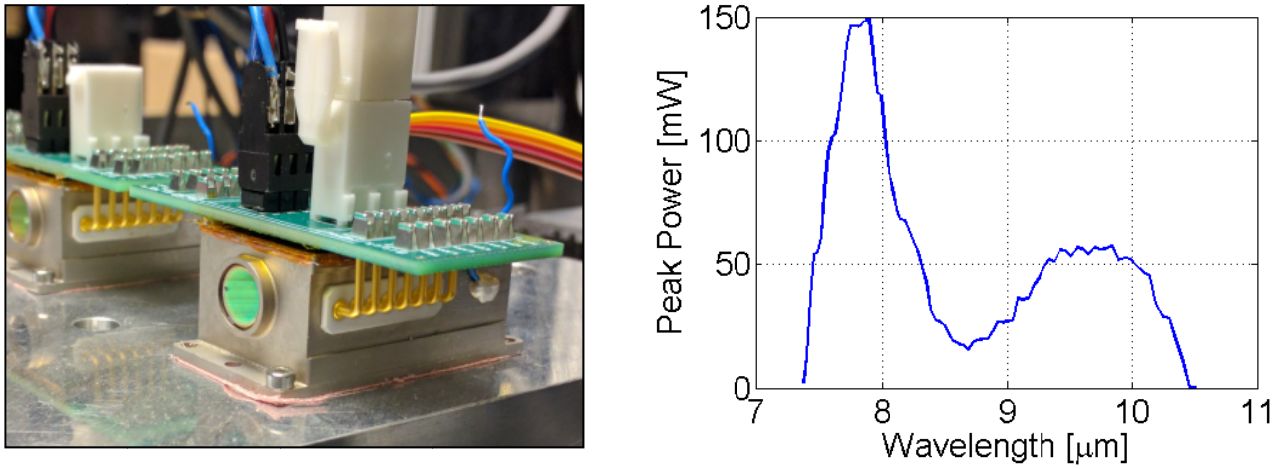

Figure 1. *Left:* Block's Mini-QCL™ is a small, rapidly tunable external-cavity QCL. *Right:* Power spectrum of QCL used in system, measured at 5% duty cycle with 50-ns pulses.

2. HYPERCUBE CAPTURE

2.1 HSI system hardware

Our system is currently based on a single Mini-QCL™ EC-QCL from Block Engineering as shown in Figure 1. The laser is tunable from 7.5 to 10.5 μm with a spectral resolution of 0.02 μm. Its peak power ranges from 20 to 150 mW with a spectrum-averaged peak power of about 50 mW. Future system enhancements will include multiplexing additional lasers to increase the spectral range and incorporating lasers that can generate higher peak power.

Both laser and camera triggering are controlled by a fast digital input/output (DIO) module such that frame capture is synchronized with laser illumination for each wavelength. At each wavelength, the laser is fired in a burst comprising of 30× 100-ns-long pulses for an active time of 3 μs over a total time of 30 μs. The average illumination energy per wavelength is thus 0.15 μJ. For image capture, the system uses a LN_2-cooled MCT focal-plane array (FPA) with 40 μm pixels which is capable of capturing 128x128 pixel frames at up to 1600 frames per second. The integration time for the camera at each wavelength is 35 μs. Table 1 details the optical configuration of the HSI system for the measurements given in this paper.

During measurement, the HSI system scans the full spectrum of the EC-QCL, capturing a total of 150 frames in 95 ms. Of those frames, 137 are during laser illumination (each frame at a different wavelength) and 13 are 'dark' frames without laser illumination. The dark frames are used to measure the thermal background. We believe this is the fastest capture of a laser-based MIR hypercube to date.

For measurement of larger surfaces, the system has an integrated two-axis galvanometer-based scanning mirror system (scanner) with a step response of roughly 250 μs to raster scan the laser illumination across the surface to fill the entire camera field of view. Raster scanning also allows us to choose a smaller beam size (and thus higher average fluence) at the expense of a longer total capture time.

Table 1. Measurement configurations for close and long range measurements.

	Close range	*Long range*
Standoff Distance	60 cm	5 m
Camera Lens	50 mm, f/2	200 mm, f/2
Camera field of View	60 mm	120 mm
Spatial Resolution at Target	0.4 mm	1 mm
$1/e^2$ Beam Diameter at Target	1 cm	3 cm
Laser illumination angle	10 deg	1 deg
Sample angle	0 deg	0 deg

2.2 Hypercube generation

The target is illuminated at non-normal incidence to measure the diffuse surface reflectance. The reflectance of the target is measured relative to that of a sandblasted aluminum reference sample. Our final result is a reflectance hypercube, obtained by taking the ratio of the intensity hypercubes from the target of interest and the reference target.

As shown in Figure 2, thermal background is subtracted from each frame of the measured hypercube to isolate the signal due to laser illumination. This is performed for both the target sample and a reference diffuse reflector. The hypercube of the reference diffuse reflector is blurred to remove the effects of surface roughness and speckle, creating a map of laser illumination intensity. The hypercube of the target sample is then divided by that of the reference reflector to yield a reflectance spectrum. This method of presentation removes the spectral effects of the laser, optics, and camera, giving a data set that only involves the spectral information of the sample.

For raster-scanned targets, a hypercube is captured at each scanner position. These individual hypercubes are then intelligently combined into a single composite hypercube.

3. SAMPLE PREPARATION

There are two general classes of samples measured: solids and liquids. Liquid samples are typically dispensed via pipette onto the chosen substrate and may then be mechanically spread for uniformity. Solid samples are prepared in two different ways. ‘Particulate’ samples are prepared via sifting particles onto a surface, typically glass. ‘Solution deposited’ samples are prepared via solution deposition in which the target chemical is dissolved in a volatile organic solvent and then airbrushed onto the substrate. With solution-deposition, the slow evaporation of the solvent often leads to crystallization of the solid. Examples of the two different chemical morphologies can be seen in Figure 4.

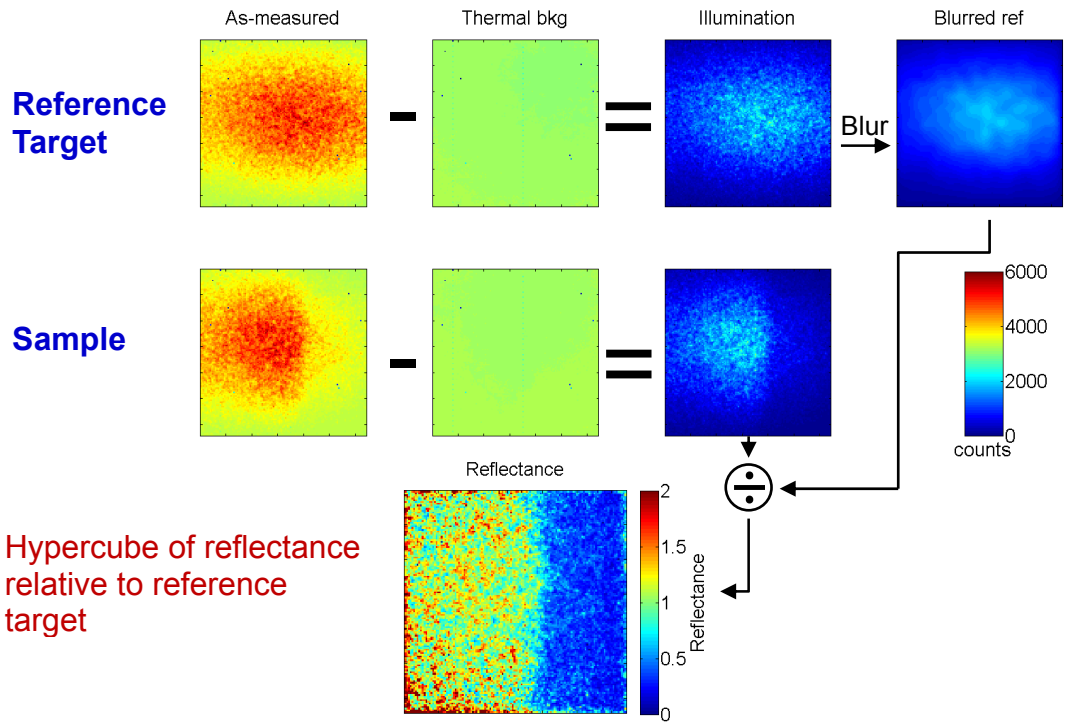

Figure 2. Data processing for generating hypercubes. First, the thermal background is subtracted from the sample and reference measurements. Then, the reference measurement is blurred to create a map of the illumination intensity. The sample is then divided by the reference to create a reflectance hypercube.

4. RESULTS

Measurements have been made of a large number of samples using the HSI system. Only a few examples are given here.

4.1 Liquid measurements

Figure 3 shows the spectral reflectance of silicone oil on both sandblasted aluminum and rough high-density polyethylene (HDPE). Measurements were made at a range of 0.6 m. Figure 4a shows a single hypercube frame of the aluminum sample with roughly 1 µL of silicone oil spread over a 0.8-cm^2 circle creating a film that is approximately 10-µm-thick. Figure 4b shows the strong, sharp absorption peak at 1260 cm^{-1} as well as broader peaks at 1025 and 1075 cm^{-1} of silicone oil. Based on the levels of absorption in the spectra, we can infer that the chemical is thicker towards the center and thinner near the edge. Figure 4c shows a hypercube frame of the HDPE sample with roughly 1 µL spread mechanically over a 2.3-cm^2 area to create a film that is approximately 4-µm-thick. Figure 4d shows the corresponding spectra which again show features at 1025, 1075, and 1260 cm^{-1}. Comparing the two measurements highlights an important difference: while the absorption lines of silicone oil cause a reduction in reflected power in the case of the aluminum substrate, they cause an increase in the reflected power from the HDPE sample. This can be attributed to the difference in optical boundary conditions at the liquid-substrate interface between the metallic and the dielectric substrates [7, 8].

The HSI system has also been used to measure samples at 5-m standoff, as shown in Video 1. The video shows an HDPE sample with an IARPA logo drawn in two different chemicals: triethyl phosphate (TEP) and silicone oil. The measurement also shows the effects of speckle noise, which is caused by coherent laser light reflecting off the rough surface of the HDPE.

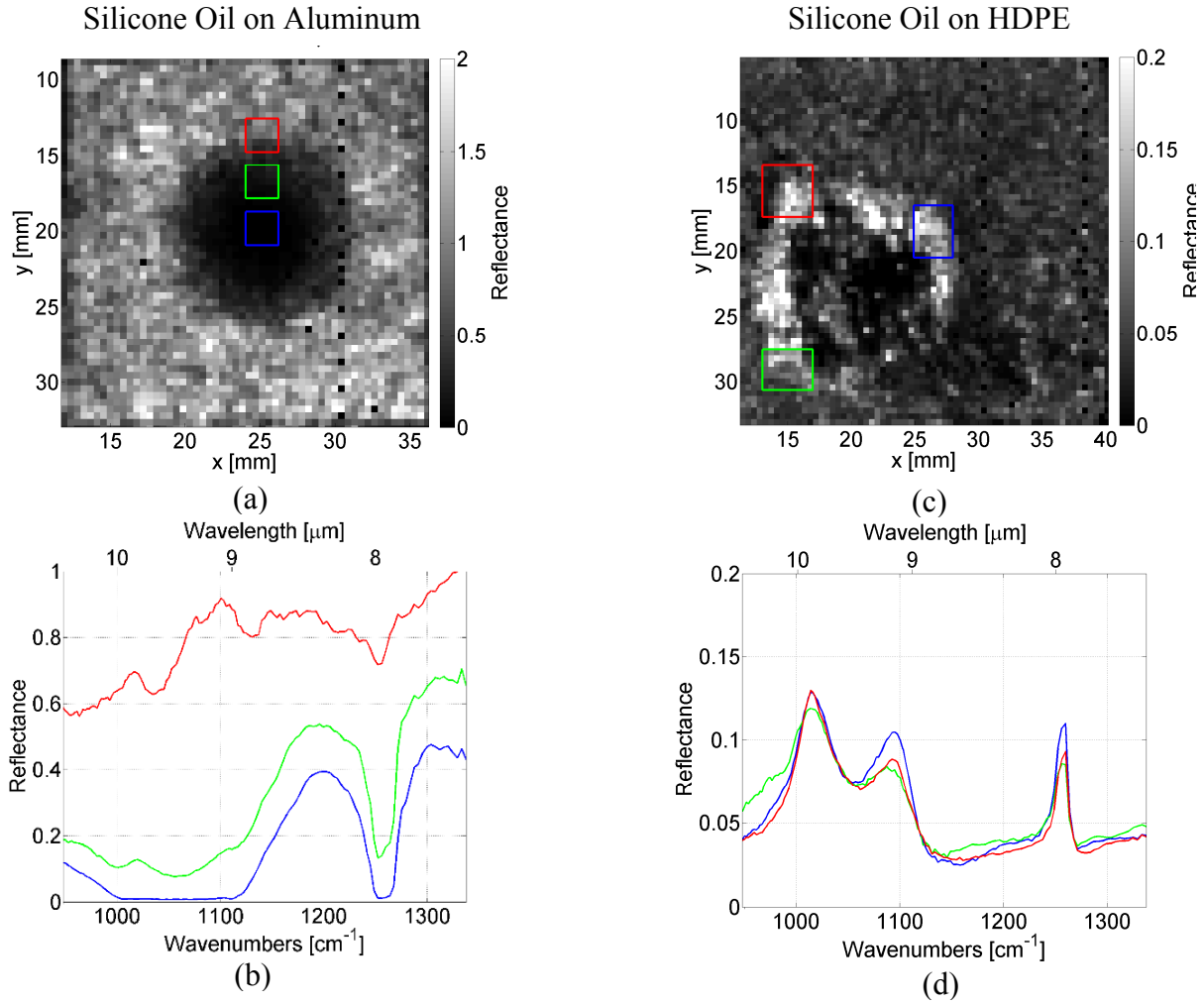

Figure 3. Results from hypercubes of silicone oil on both metallic and dielectric substrates. (a) and (b) show a single hypercube frame and some averaged spectra from a measurement of silicone oil on sandblasted aluminum at 60 cm standoff. The spectra demonstrate a thickness gradient from the center of the target to the edge. Each colored spectrum in (b) is the average of pixels highlighted in the corresponding colored box in (a). (c) and (d) show similar measurements of silicone oil mechanically spread on HDPE.

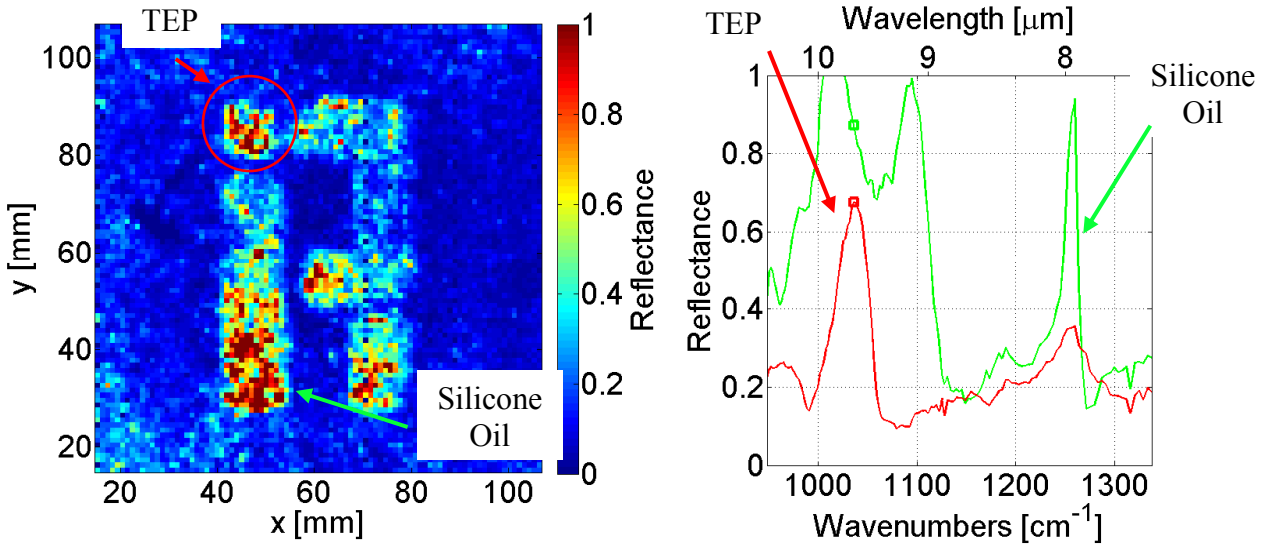

Video 1. Demonstration hypercube of an IARPA logo drawn in TEP (red spectrum) and silicone oil (green spectrum) on HDPE. Each frame of the video is captured at a different wavelength, as shown by the moving squares on the right plot. The sample was measured at 5-m standoff. http://dx.doi.org/10.1117/12.2261851.1

4.2 Solid Measurements

The HSI system has also been used to measure trace solid particles and residues on soda-lime glass substrates at a standoff distance of 0.6 m. Figure 4 compares the morphology and spectra of two samples of caffeine on glass which have been prepared in different ways: "particulate" and "solution-deposited." The particulate sample has 24 μg/cm^2 of caffeine with a median diameter of 10 μm, sifted onto a 2.5 x 2.5 cm^2 substrate. The solution-deposited sample has an evenly-distributed film with a loading of 76 μg/cm^2 on a 10 x 10 cm^2 substrate. The solution-deposited sample clearly has a crystalline structure when viewed under a microscope.

The two samples have noticeably different spectra. The particulate sample gives a spectrum which is very similar to the product of the spectrum of bulk caffeine and the spectrum of glass with dips in the reflection spectrum corresponding to the imaginary part of the refractive index of caffeine. The solution-deposited sample shows dispersive effects, mirroring the shape of the real part of the index of refraction. The solution deposited sample also has a higher reflectance from 1250 to 1350 cm^{-1} which is indicative of a diffuse first surface reflection as opposed to the specular behavior expected from a smooth piece of glass. This comparison highlights the spectral differences which can occur in real-world detection situations.

Figure 5 shows two spectra measured for particulate samples of acetaminophen and RDX on 2.5 x 2.5 cm^2 glass substrates. Overlaid with the measurements are results of a simple signature model. The total reflection spectrum R_{target} is calculated based on three different paths the incident light can take. The first term is the direct reflectance from the substrate, R_{sub}. The second term is the back reflectance R_{powder} from the particles. The third term is the light that scatters off both the particle and the substrate. These factors are applied using the particle fill factor, *FF*, and two fit parameters C_{back} and C_{fwd} [7]. Considering its simplicity, this model gives surprisingly good correspondence with measurements. We plan to further refine the model to achieve even better correspondence with measurements.

$$R_{target} = (1 - FF)R_{sub} + FF\left(C_{back} + C_{fwd}R_{sub}\right)R_{powder}$$

Figure 6 shows the measured reflectance of samples of RDX on glass with the mass loading ranging over nearly two orders of magnitude. A few observations can be drawn from this measurement. The shape of the spectra is preserved as the loading is changed. Also, the reflectance scales roughly linearly with mass loading. The existing setup can measure

particle loadings of <1 μg/cm^2 on glass. As higher power lasers are installed in the system, this limit should go down proportionally.

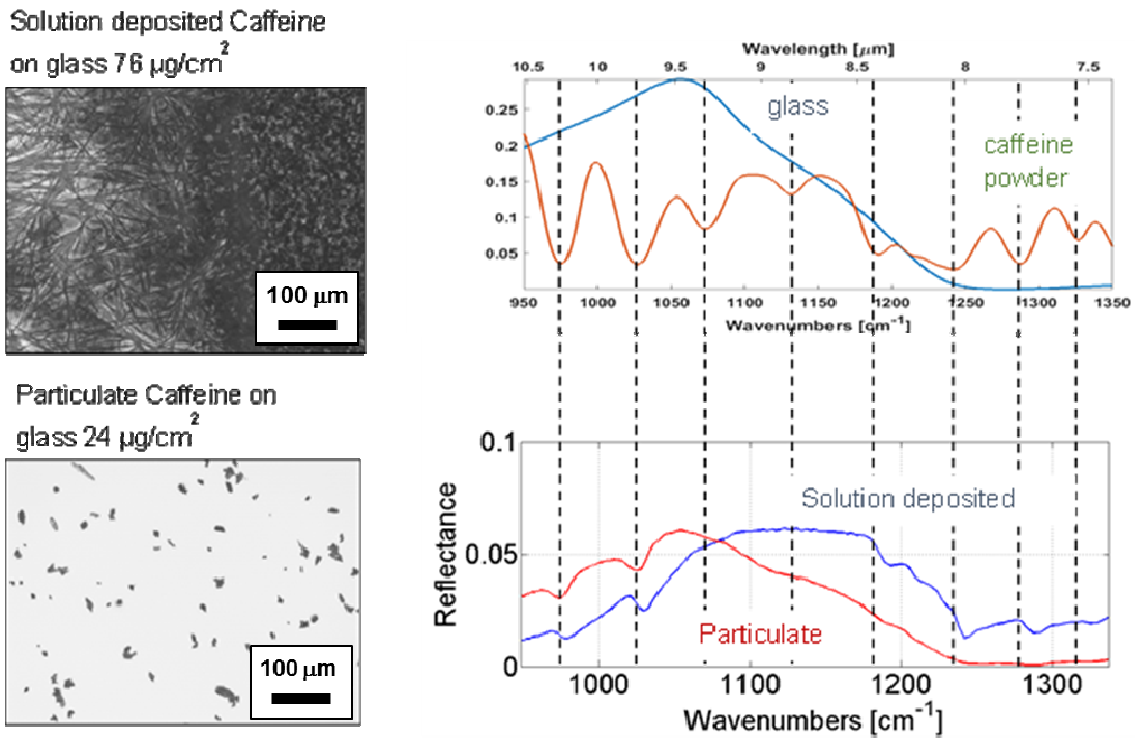

Figure 4. Comparison between particulate and solution-deposited caffeine on glass. Photomicrographs on the left clearly indicate morphological differences between crystalline structure of the solution-deposited and the particulate samples. The plots on the right show the effects of those morphological differences in hypercubes captured at 60 cm standoff. The particulate sample gives a spectrum that is very close to the product of the bulk powder measurement and glass. The deposited sample, on the other hand, shows dispersive spectral features that mirrors the shape of the real part of the chemical's refractive index.

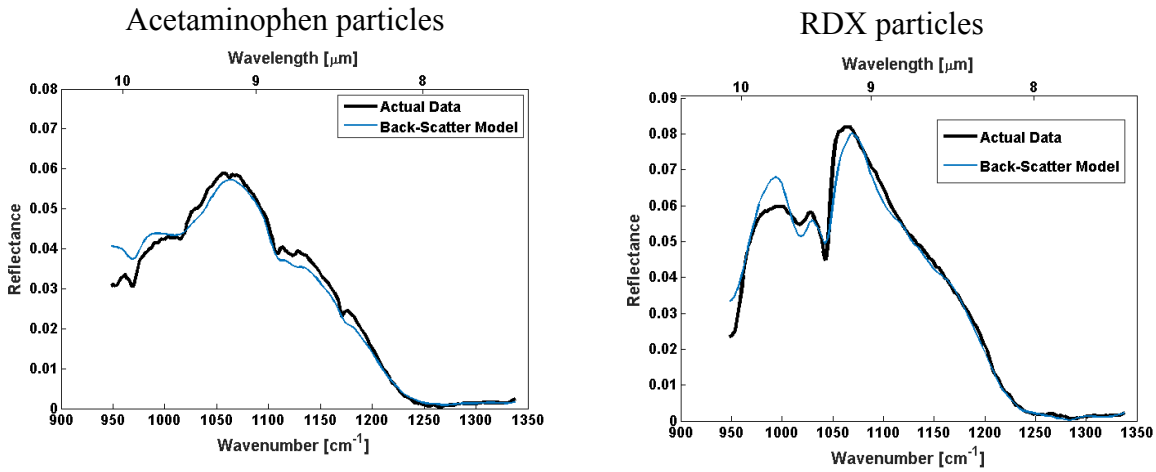

Figure 5. Measured spectra of particulates of acetaminophen (left) and RDX (right) on glass. Each spectrum is the average of roughly 1000 pixels from the hypercube captured at 60 cm standoff. Also plotted are the modeled spectra using the simple signature model.

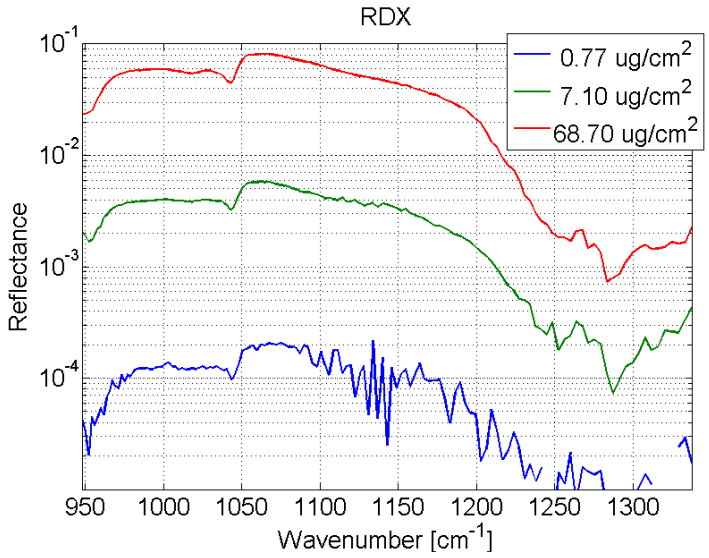

Figure 6. Reflection spectra of RDX particles on glass at different loadings. Particle fill factors from lowest to highest loadings are 0.05%, 0.4%, and 4%. Displayed spectra are averaged over roughly 1000 pixels.

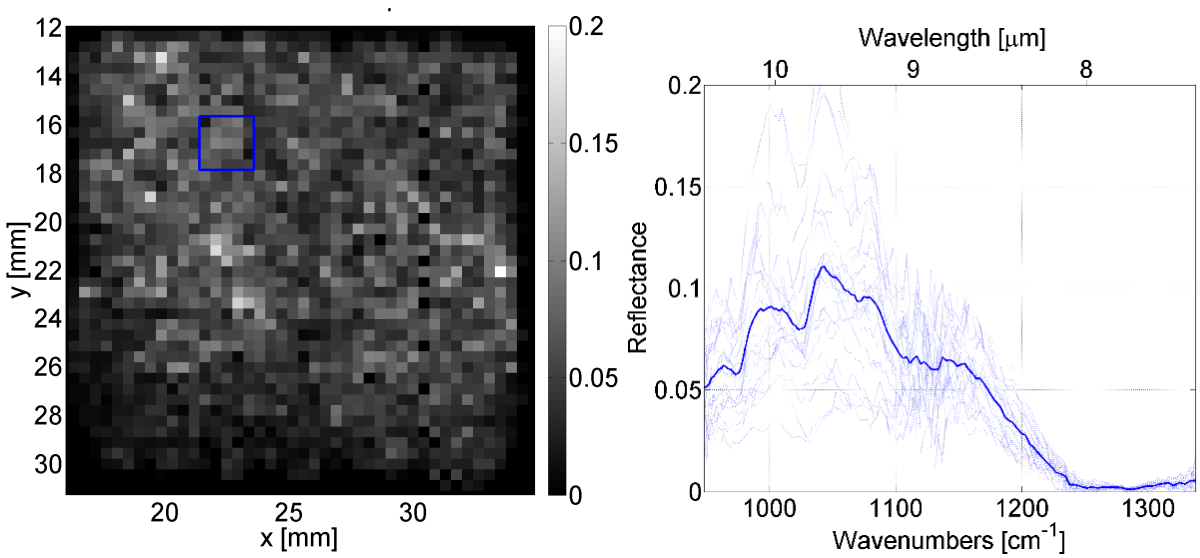

Figure 7. Hypercube of particulate caffeine on glass. Individual pixels show significant variation. The left plot displays individual spectra and the average from the area highlighted on the left. Spectra from 25 pixels are displayed.

Figure 7 displays some of the pixel-to-pixel variation seen in measured hypercubes. We attribute these variations to a combination of particle size variation, particle distribution inhomogeneity, and speckle from the rough surface of the particulate itself. As shown in Figure 8, the variability seems to be mostly in magnitude and not in spectral similarity. The angular spectral variability, *cos θ*, is calculated as a normalized dot product between the spectrum of each pixel and the average of all pixels. This is the basic concept used in the ACE detection algorithm. The magnitude is simply the normalized spectral magnitude for each pixel.

$$\cos\theta = \frac{\bar{S}\cdot\langle\bar{S}\rangle}{|\bar{S}|\cdot|\langle\bar{S}\rangle|}; \qquad Magnitude = \frac{|\bar{S}|}{|\langle\bar{S}\rangle|}$$

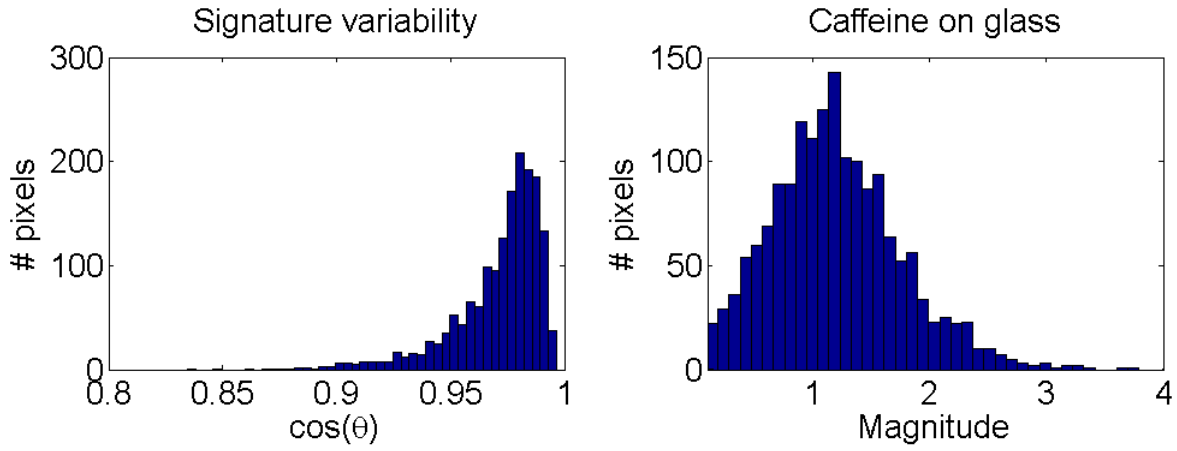

Figure 8. Spectral variability of pixels compared to sample average. There is much larger fluctuation in magnitude than in cos θ. Sample is particulate caffeine on glass.

5. CONCLUSIONS

We present results from a hyperspectral imaging system that accurately and rapidly captures hypercubes using EC-QCLs. It can capture hypercubes with 137 illumination frames and 13 dark frames in 95 ms. To the best of our knowledge, this is the fastest hypercube capture using wavelength tunable lasers in the MIR. The system was used to investigate a range of samples with different morphologies and different mass loadings, including silicone oil on Aluminum and HDPE and assorted solids on glass. Solid particles on glass were measured with mass loadings below 1 $\mu g/cm^2$. Investigations continue to refine signature models and to understand the effects of signature variability and speckle in measured spectra.

6. ACKNOWLEDGEMENTS

We gratefully acknowledge the support of the IARPA SILMARILS program through AFRL contract FA8650-16-C-9107. We also thank the Applied Physics Laboratory at Johns Hopkins University (JHU/APL) and the Naval Research Laboratory (NRL) for providing samples and to the Pacific Northwest National Laboratory (PNNL) for providing reference spectral data.

REFERENCES

[1] A. K. Goyal and T. R. Myers, "Active mid-infrared reflectometry and hyperspectral imaging", chapter in [Laser-Based Optical Detection of Explosives] CRC Press (2015).
[2] Goyal, A. K., et al., "Active infrared multispectral imaging of chemicals on surfaces," Proc. SPIE 8018, 80180N (2011).
[3] Goyal, A. K., et al., "Active hyperspectral imaging using a quantum cascade laser (QCL) array and digital-pixel focal plane array (DFPA) camera," Opt. Express 22, 14392 (2014).
[4] Ostendorf, R., et al., "Recent Advances and Applications of External Cavity-QCLs towards Hyperspectral Imaging for Standoff Detection and Real-Time Spectroscopic Sensing of Chemicals," Photonics, 3(2), 28 (2016).
[5] Faist, J. [Quantum Cascade Lasers], Oxford University Press: Oxford, UK, (2013).
[6] Caffey, D., et al., "Performance characteristics of a continuous-wave compact widely tunable external cavity interband cascade lasers," Opt. Exp. 18(15), 15691 (2010).
[7] Myers, T. R., et al., "Mid-infrared hyperspectral scene simulator for laser-based detection of trace chemicals on surfaces," Proc. SPIE 10198 (2017).
[8] Raz, G., et al., "Novel Trace Chemical Detection Algorithms: A Comparative Study," Proc SPIE 10198 (2017).